Southern Ocean contributions to the Eastern Equatorial Pacific heat content during the Holocene

Julie Kalansky[1,2*], Yair Rosenthal[1], Timothy Herbert[3], Samantha Bova[3] and Mark Altabet[4]

[1]*Institute for Marine and Coastal Sciences, and Department of Earth and Planetary Sciences, Rutgers University, 71 Dudley Road, New Brunswick, NJ, 08901, USA*

[2]*Scripps Institution of Oceanography, University of California, 9500 Gilman Drive, 9500 Gilman Drive, La Jolla, California, 92093, USA*

[3]*Department of Earth, Environmental, and Planetary Sciences, Brown University, Providence, RI, 02921, USA*

[4] *School for Marine Science and Technology, University of Massachusetts Dartmouth, New Bedford, MA, 02747, USA*

[*]*Corresponding author (Scripps Institution of Oceanography, University of California, 9500 Gilman Drive, 9500 Gilman Drive, La Jolla, California, 92093, USA*; jkalansky@ucsd.edu)

Southern Ocean contributions to the Eastern Equatorial Pacific heat content during the Holocene

Abstract

Temperature reconstructions from a shallow core (375 m) from the Peru Margin are used to test the influence of Subantarctic Mode Water (SAMW) on the eastern equatorial Pacific (EEP) thermostad and thus the effect of southern high latitude climate on interior ocean heat content (OHC). Temperature estimates, based on Mg/Ca measurements of planktonic and benthic foraminifera (*Neogloboquadrina dutertrei* and *Uvigerina spp.*, respectively) show higher temperatures in the early Holocene, a cooling of ~2° by 8 kyr B.P. and after relatively stable temperatures to the present. The temperature signal is similar in direction and timing to a rather robust Holocene climate signal from the southern high latitudes suggesting it originated there and was advected to the core site in the EEP. Based on the *N. dutertrei* and *Uvigerina* Mg/Ca temperature and $\delta^{13}C$ records we conclude that SAMW acted as a conduit transporting the southern high latitude climate to the interior of the equatorial Pacific. We propose that the early Holocene warmth is related to a southward migration of the Subtropical Front, which enhanced the influence of warm subtropical water in the region of SAMW formation and was then transported to the EEP thermostad. The early Holocene warmth recorded in the EEP thermostad has a muted sea surface temperature expression indicating this mechanism is important for sequestering heat in the ocean interior.

1. Introduction

Interior ocean heat content (OHC) is an important component of the climate system as it sequesters excess energy and mitigates the effects of a changing climate [*Levitus et al., 2012*]. While the recent plateau in global temperature over the past decade has brought increased attention to the role of OHC in climate change, the mechanisms and locations by which heat enters and spreads in the ocean interior are debated [*Balmaseda et al.*, 2013]. Strengthening of equatorial trade winds has been argued to account for the recent increase in OHC [*England et al.*, 2014], as have changes in the Atlantic Meridional Overturning Circulation [*Balmaseda et al.*, 2013] and changes in the location of the Southern Westerly Winds (SWW) [*Roemmich et al.*, 2015]. Additionally, modeling studies suggest that the Southern Ocean is important in controlling OHC due to the outcropping of intermediate and deep isopycnal layers that transport water into the interior ocean [*Cai et al.*, 2010]. The impact of the Southern Ocean on OHC might be particularly relevant on centennial and longer time scales because the response of density structures is greater than 100 years due to the coupling with changes in the northern high latitudes [*Jones et al.*, 2011]. Supporting the influence of the Southern Ocean on OHC on millennial timescales, a recent study by Rosenthal et al. [2013] argues that Holocene changes in equatorial Pacific OHC originated both in the northern and southern high latitudes, however, the evidence for a link to the Southern Ocean is tenuous.

A rather robust change of southern high latitude climate during the early Holocene allows us to test the extent that the Southern Ocean influences low latitude Pacific OHC on centennial to millennial time scales. Several different reconstructions suggest that the southern high latitudes were warmer prior to 8 kyr B.P. Sea surface temperature (SST) records from the southwest Pacific show warmer temperatures during the early Holocene followed by a cooling at 8 kyr, which has been attributed to a southward location of the Subtropical Front (STF) [*Bostock et al.*, 2013, and references within]. The southern position of the STF was likely a basin wide adjustment as SST on the eastern side of the south Pacific, at 41˚S, also show a similar temperature trend [*Kaiser et al.*, 2005]. The early Holocene warmth has also been documented further south near the West Antarctic Peninsula [*Shevenell et al.*, 2011]. Ice core $\delta^{18}O$ reconstructions of Antarctic air temperatures also suggest warmer temperatures between ~11-10 kyr B.P. and cooling by ~8.5 kyr B.P. [*Masson-Delmotte et al.*, 2011; *Mulvaney et al.*, 2012]. Furthermore, records from southern Chile indicate increased precipitation prior to 8 kyr B.P due to strong SWW in the core of the wind belt [*Lamy et al.*, 2010]. These early Holocene changes have variably been attributed to orbital forcing [*Masson-Delmotte et al.*, 2011; *Shevenell et al.*, 2011], changes in the intensity and location of the SWW [*Lamy et al.*, 2010; *Shevenell et al.*, 2011] and the bipolar seesaw [*Lamy et al.*, 2010].

To affect the low latitude OHC in the upper 400 m, the Southern Ocean change at 8 kyr B.P. most likely propagated via Subantarctic Mode Water (SAMW). SAMW forms in the Southern Ocean north of the Subantarctic Front [*Hartin et al.*, 2011] during the winter when mixed layers can exceed 400 m and transports heat, salinity, and nutrients from the southern high latitudes equatorward [*Herraiz-Borreguero and Rintoul*, 2011; *Spero and Lea*, 2002]. A model tracer experiment suggests that SAMW is likely a major contributor to the equatorial Pacific thermostad (~150-300 m) [*Qu et al.*, 2009], also referred to as the 13˚C Water [*Tsuchiya*, 1981]. Additionally, radiocarbon ($\Delta^{14}C$) data from the Peru margin and Holocene $\delta^{13}C$ reconstructions from the eastern equatorial Pacific (EEP), suggest that SAMW reaches the equator [*Spero and Lea*, 2002; *Toggweiler et al.*, 1991]. However, modern Argo float data suggest that SAMW temperature and salinity signals do not extend beyond 30˚S in the Pacific [*Herraiz-Borreguero and Rintoul*, 2011]. The difference between the Argo float and the carbon isotope data is likely because temperature is an active tracer, meaning it affects the fluid properties, whereas the carbon isotopes are passive tracers. However, if the temperature signal in SAMW was sufficiently strong, the carbon isotopes imply it could reach the thermostad impacting the interior OHC in the equatorial region. Here, using paleotemperature reconstructions in a core from the northern Peru margin we provide further evidence that the SAMW is a major conduit of southern high latitude climate signals and test the hypothesis that the southern high latitudes influence low latitude OHC on millennial timescales.

2. Oceanographic Setting

The temperature reconstructions are from the upper and lower limit of the EEP thermostad. The thermostad is a depth interval of relatively uniform temperature below the Pacific Equatorial Undercurrent (EUC) [*Tsuchiya*, 1981] and arguably originates from SAMW, although other possible origins include the southeast Pacific and northeast of New Zealand [*Qu et al.*, 2009; *Spero and Lea*, 2002; *Toggweiler et al.*, 1991]. Assuming SAMW is a major contributor to the thermostad water, the pathway from the Southern Ocean to the EEP is likely via the New Guinea Coastal Undercurrent. In the Pacific basin, once SAMW subducts it travels northwestward with some SAMW reaching the Solomon Sea near Papua New Guinea [*Herraiz-Borreguero and Rintoul*, 2011] and then it likely enters the New Guinea Coastal Undercurrent. This is also supported by tracer model experiments which show that the thermostad originate in SAMW formation regions but enters the equatorial region through the Western Boundary Currents [*Qu et al.*, 2009]. The water then travels eastward across the equatorial pacific to reach the EEP. A tracer experiment study suggests that the thermostad water eventually upwells to the surface in the Peru cold tongue possibly communicating signals from outside the equatorial region to the surface [*Qu et al.*, 2010], however, whether or not the subsurface temperature from the thermostad influences SST has not been proven.

The equatorial Pacific thermostad extends between approximately 5˚N to 5˚S and is characterized by a temperature range of 11-14˚C and density of σ_θ = 26.2-26.65 kg/m^3 [*Tsuchiya*, 1981]. The thermostad is bounded to the north and south by the subsurface counter currents (SSCC) with the thermostad becoming wider and thicker in the east. In the western equatorial Pacific the thermostad is found between ~225-275 m whereas in the east it is between ~150-300 m (Figure 1). The formation and the thickening of the thermostad has been attributed to the mixing at the base of the EUC, due to the high shear from the current [*Toggweiler et al.*, 1991] and through diapycnal fluxes along the SSCC [*Rowe et al.*, 2000]. Mixing of warmer water along the EUC explains how higher density SAMW (σ_θ = 26.9–27.15 kg/m^3) can be transformed into the warmer, less dense water of the thermostad [*Toggweiler et al.*, 1991].

3. Methods

We have reconstructed the temperatures close to the top and the base of the EEP thermostad using giant piston core KNR195-5 CDH23 from the Peru Margin in the EEP (3˚45'S, 81˚08'W, 374 m water depth, 1715 cm) (Figure 2). The temperature reconstructions are based on Mg/Ca measurements in *Neogloboquadrina dutertrei*, a thermocline dwelling planktonic foraminifer and *Uvigerina spp.*, an infaunal benthic foraminifer. In the EEP, *N. dutertrei* calcifies between 75-150 m [*Rincon-Martinez et al.*, 2011], which is below the shallow thermocline. *Uvigerina* is usually found in the first 1-2 cm of the sediment, such that it records bottom water temperature. The σ_θ (relative to the modern surface) values of the two water masses being reconstructed are 26.1 and 26.7 kg/m^3, for *N. dutertrei* and *Uvigerina* respectively, and are associated with the density surface just above and below the thermostad (Figure 1).

3.1 Age Model

The age model for CDH23 is based on 17 radiocarbon dates from *N. dutertrei* (Table 1) and converted to calendar age using a reservoir age of 500 years and the Fairbanks et al. [2005] calibration. The age model was calculated by linearly interpolating between radiocarbon dates; the age reversal was accounted for by averaging the dates at 850 and 900 cm and using a depth of 875 cm. The average sedimentation rate for the core is about 100 cm/kyr (Figure 3) and it was sampled at 8 cm, ~80 year, intervals. All ages reported here are thousand years before present (B.P.).

3.2 Analysis

Between 15-20 tests of *N. dutertrei* from 355-425 µm size fraction and 10-15 *Uvigerina spp*. specimens from greater 200 µm were split for isotope and trace metal analysis. However, *Uvigerina* abundance decreased between 600-750 cm in the core only permitting either trace metal or isotope measurements due to limited material. For trace metal analysis, foraminifera were cleaned using the reductive-oxidative method of Rosenthal et al. [1997]. The samples were dissolved in 100 µL of 0.065 M HNO_3 and diluted with 300 μL of 0.5 N HNO_3, such that the final calcium concentrations ranged from 1-5 mM.

Trace metal ratios were determined at Rutgers University, using a Thermo Finnigan Element XR sector-field inductively coupled plasma mass spectrometer (ICP-MS). In addition to Mg/Ca ratios we measured Al/Ca, Fe/Ca, Mn/Ca and Ti/Ca, to monitor possible contamination from oxides and silicates. Samples were matrix corrected and the Mg/Ca matrix correction was always less than 2% of the original value. Samples were then converted into mmol/mol ratios and drift corrected using a spiked gravimetric standard, which has a Mg/Ca value of 6.34 mmol/mol. The long term Mg/Ca precision (1 S.D.) for the time period of the data presented here was 0.83%, 0.71% and 0.66%, based on repeated analysis of three consistency standards of 1.44, 3.49 and 8.71 mol/mol, respectively. Samples with Mn/Ca, Fe/Ca, or Al/Ca above the 100 μmol/mol threshold, or Mg/Ca ratios higher by 2 sigma deviations than other samples in the run, were considered as possibly contaminated and eliminated. These only included 2 *Uvigerina* and no *N. dutertrei* samples.

Carbon and oxygen isotope analyses were preformed at Rutgers University on a Micromass (FISONS) Optima Isotope Ratio Mass Spectrometer. The samples were drift corrected if necessary using an in house standard. The standard is run against the international NBS19 biannually. Throughout all the runs the standard deviation was ±0.05‰ for $\delta^{13}C$ and ±0.1‰ for $\delta^{18}O$. Isotope values are reported in PDB. The $\delta^{18}O$ of calcite was corrected for sea level by fitting a polynomial to coral sea level data [*Bard et al.*, 2010; *Lighty et al.*, 1982; *Peltier and Fairbanks*, 2006] and then assuming a 0.1‰ change in $\delta^{18}O$ per 10 meters of sea level change.

3.3 Temperature Calibrations

Discrete $\delta^{18}O$ of seawater ($\delta^{18}O_{sw}$) measurements from a CTD cast conducted during the coring cruise were converted to $\delta^{18}O$ of carbonate ($\delta^{18}O_c$) values using the linear Marchitto et al. [2014] *Uvigerina* equation, ($\delta^{18}O_c$ - $\delta^{18}O_{sw}$)= -0.231±0.004T + 4.03±0.03. Of the different calibration equations tested, most planktonic calibrations produced $\delta^{18}O_c$ profiles that were too deplete and did not intersect measured *N. dutertrei* $\delta^{18}O_c$ values (Supplemental Figure 1). Of the calibration equations that were in range of the measured *N. dutertrei* $\delta^{18}O_c$ values this equation was the most robust. Based on the comparison with core top *N. dutertrei* $\delta^{18}O_c$ values we estimated the calcification depth of *N. dutertrei* to be at approximately 100 m (Figure 4), slightly shallower than the top of the thermostad. Using the multi-species planktonic Mg/Ca calibration of Anand et al. [2003] we obtain a subthermocline temperature of 14.7±1.3˚C, which is within the measured modern temperature at 100 m (14.9˚C). The standard error (SE) on the absolute temperature includes errors in the core top measurements and the calibration. The error in estimating the downcore temperature anomaly, calculated relative to the average temperature between 1850-1880 Common Era, is reduced to ±1.1˚C because it only relates to the slope of the calibration. Using a three point running average further reduces the error on the temperature anomaly to ±0.8˚C.

Uvigerina core top calibrations provide a range of sensitivities as reviewed in Bryan and Marchitto [2008]. All the available calibrations produce temperatures that are 2-6˚C colder than the bottom water temperature at the core site. Because there are insufficient core tops from the Peru Margin to produce a regional calibration, we used the linear calibration from Bryan and Marchitto [2008] (Mg/Ca = (0.7±0.05) + (0.084±0.005)*T) and adjusted the intercept to fit the bottom water temperature. This calibration was chosen because it includes much of the published core top data. However, to match the bottom water temperature at the core site of 10˚C the intercept was adjusted to 0.26, which is significantly lower than observed elsewhere. Differences in *Uvigerina* calibrations due to location have been previously recognized with a Pacific calibration having a lower slope than an Atlantic calibration [*Martin et al.*, 2002]. It has been argued that *Uvigerina* is not affected by saturation state since it is an infaunal species [*Elderfield et al.*, 2010]. At this point we can only hypothesize that low carbonate concentrations in the pore waters of the low %$CaCO_3$ sediment underlying the strong upwelling region of the Peru Margin may impact Mg/Ca values. Previous studies have suggested using Li/Ca of *Uvigerina* rather than Mg/Ca to account for the impact of carbonate saturation [*Bryan and Marchitto*, 2008]. Using Li/Ca values on the core tops produced temperatures that were ~2˚C too cold, however, since this has not been tested in a robust manner, and there were not sufficient core tops to generate a Li/Ca calibration, we concluded using an adjusted Mg/Ca *Uvigerina* calibration was the most sound approach. The difference between the original and adjusted equations is 5.2˚C, with core tops averaging 4.0˚C using the original equation and 9.2˚C using our adjusted equation.

Given that this region was under similar condition for the past 10,000 years, we assume that the sensitivity and intercept of the calibration were constant throughout the Holocene, which is generally supported by the comparison with the *N. dutertrei* temperature record. Hence in estimating the temperature anomalies we only consider the error in the slope. The standard error associated with the *Uvigerina* temperature estimates is ± 1.8˚C, whereas the error of the temperature anomaly is ± 1.6˚C and the error of the 3-point running average smoothed data is ± 1.1˚C. The *Uvigerina* temperature estimates were corrected for sea level change using the sea level curved mentioned in section 3.2 and an approximated temperature gradient of 1˚C per 60 m based on temperature profiles from the cruise (See Supplemental Figure 2 for comparison). This corrects for the assumption that as sea level increased throughout the Holocene, the benthic temperature would decrease solely due to the core becoming deeper. The difference between the corrected temperature data and uncorrected data is greatest at the beginning of the record, 0.8˚C, and decreased to 0.1˚C by 5 kyr. Most of the Mg/Ca temperature estimates are coherent with changes in sea level corrected $\delta^{18}O_c$ (Figure 5), supporting the sign and timing of the *Uvigerina* Mg/Ca determined temperature variations.

4. Results

Both the *Uvigerina* and *N. dutertrei* records show warmer temperatures prior to 8 kyr (Figure 5). Between 10.7 and 9 kyr the *N. dutertrei* temperature varies between 15 and 17˚C decreasing relatively rapidly to 14˚C by 8.8 kyr and then ~13˚C by 8 kyr. From 8 kyr to end of the record at 1 kyr, *N. dutertrei* temperature exhibits multicentennial temperature variability between 12 and 15˚C with no discernible long-term trend. A spectral analysis of the temperature record between 8 kyr and 1 kyr does not indicate any significant periodicities (not shown). The sea level corrected $\delta^{18}O_c$ values vary between 0.5 and 0.3‰ from 10-9 kyr and become more enriched to 0.8‰ by 8.8 kyr indicating warmer and/or fresher thermostad waters in the early Holocene. The Mg/Ca estimated temperature change from 10-8 kyr is approximately 2.5 ±0.8˚C, whereas, assuming there is no change in the $\delta^{18}O_{sw}$, the $\delta^{18}O_c$ indicate about a 1.3±0.4˚C temperature change. The difference between the $\delta^{18}O_c$ and Mg/Ca temperature estimates implies salinity increased during this period.

Uvigerina determined bottom water temperature varies between 11.5 and 12.5˚C from 10.7-9 kyr and decreases rapidly to 10.5˚C by 8.8 kyr. For the remainder of the record the *Uvigerina* temperature varies from 9.5-11.5˚C. Between 9.3 and 8.8 kyr the sea level corrected *Uvigerina* $\delta^{18}O_c$ becomes more enriched from 1.5 to 1.8‰ indicating a 1.7˚±0.6˚C decrease in temperature using the Bemis et al. [2002] *Uvigerina* specific equation and assuming there is no change in $\delta^{18}O_{sw}$ other than ice volume. This is within error of the Mg/Ca estimate of 2 ±1.1˚C (Figure 5). The Bemis et al. [2002] equation was used rather than the Marchitto et al. [2014] equation because for *Uvigerina* because the Bemis et al. [2002] equation estimates more accurate bottom water temperatures from Peru Margin core top (data not shown).

The $\delta^{13}C$ of *Uvigerina* and *N. dutertrei* increase during the Holocene (Figure 5). The $\delta^{13}C$ of *N. dutertrei* increases from ~1 to 1.4‰ and the *Uvigerina* $\delta^{13}C$ increases from -0.4 to 0.1‰ by 6 kyr. During the remainder of the Holocene *N. dutertrei* $\delta^{13}C$ varies between ~1.25 and 1.45‰ and the $\delta^{13}C$ of *Uvigerina* varies between 0 and 0.2‰.

5. Discussion

5.1 Origin of the Temperature signal

N. dutertrei and *Uvigerina* are at the upper and lower limits of the modern day thermostad, and thus the similarity between the two records in the early Holocene suggests that the temperature signal is representative of the thermostad. The early

Holocene warmth and subsequent cooling recorded in both the *Uvigerina* and *N. dutertrei* records is similar in timing to temperature records from the southern high latitudes (Figure 6). This suggests that the early Holocene warming in the EEP subsurface originated from the Southern Hemisphere. We suggest that the main conduit of this temperature signal was the SAMW rather than changes in regional winds or transported from other thermostad formation locations.

If the temperature signal was communicated to the subsurface through changes in regional winds, there would likely be a surface signal through changes in the Intertropical Convergence Zone (ITCZ) location or SST. The along shore winds in the region are stronger when the ITCZ is farther north which increases upwelling and cools SST. Reconstruction of the ITCZ location does not suggest a pronounced shift in the ITCZ at 8 kyr, but rather a northward migration beginning around 10 kyr [*Haug et al.*, 2001], which would cause cooler SST due enhanced upwelling. Further, SST records from around the region do not show a cooling between 9 and 8 kyr [*Koutavas and Sachs*, 2008; *Pena et al.*, 2008]. Thus we conclude that the Holocene subsurface temperature signal was not a result of changes in regional winds.

Modeling studies indicate the subthermocline water in the EEP is traced to the subtropics on 20-30 year time scales [*Qu et al.*, 2009] and thus may be the origin of the early Holocene warmth. If subtropical surface waters are the origin of the warmth in the early Holocene they should be warmer during this period, but this is not reproduced in the proxy records. Records from 33-36˚S off Chile do not indicate a coherent pattern of SST change between 10 and 8 kyr [*Mohtadi et al.*, 2008]. Further SST reconstruction from the subtropical north Pacific (25˚N) shows warmer SST from ~12-11 kyr, but it cools by 10 kyr [*Marchitto et al.*, 2010]. These SST records do not support that the early Holocene thermostad signal was transported from the subtropics.

Similarly, other source regions for the thermostad, off northeastern New Zealand and off southern Chile, are not the likely origin of the thermostad temperature signal either. An alkenone SST reconstruction from a core located of northeastern New Zealand, (MD-2121) shows continual warming throughout the early Holocene [*Pahnke and Sachs,* 2006] in contrast to the cooling seen in the thermostad at 8 kyr. Another possibility of the origin of the early Holocene warmth is off the coast of southern Chile, close to the modern formation site of AAIW. The water would then likely be transported along the narrow shelf along Chile and Peru. Records of SST from along the South American shelf do not show a similar warm early Holocene indicating the temperature signal would have been transported in the subsurface [*Chazen et al.*, 2009; *Mohtadi et al.*, 2008]. The Chile-Peru Deep Coastal Current is northward flowing, however the current is typically deeper than 300 m [*Chaigneau et al.*, 2013]. If this current were the main conduit of the Southern Ocean temperature signal, we would expect a larger temperature change in the *Uvigerina* data compared to the *N. dutertrei* data, which is not seen in the data. Based on these south Pacific temperature records, we conclude that SAMW is the most likely source of the early Holocene warmth recorded in the EEP thermostad.

Additionally, $\delta^{13}C$ and εNd support a Southern Ocean origin of the EEP thermostad signal. The increasing $\delta^{13}C$ values until 6 kyr in both the *N. dutertrei* and *Uvigerina* $\delta^{13}C$ are reproduced throughout the subtropical and equatorial oceans suggesting these trends likely have a common origin rather than reflecting local changes in productivity (Figure 7). Spero and Lea [2002] hypothesized that changes in Southern

Ocean $\delta^{13}C$ is transported to intermediate and thermocline waters via SAMW and AAIW. The $\delta^{13}C$ increase from the early Holocene to about 6 kyr is a rather robust feature and seen in several $\delta^{13}C$ reconstructions. The gradual increase in $\delta^{13}C$ is attributed to reinvigorated North Atlantic Deep Water contributing lower nutrient and higher $\delta^{13}C$ water and an increase in the $^{12}CO_2$ being taken up by the terrestrial biosphere [*Spero and Lea*, 2002]. The *N. dutertrei* thermocline $\delta^{13}C$ record from ODP 1240 indicates the feature is common to the equatorial Pacific subsurface [*Pena et al.*, 2008]. A similar signal is documented in the $\delta^{13}C$ of *G. ruber* in the Arabian Sea [*Sirocko et al.*, 1993] and in both *G. ruber* and *G. inflata* in the southwest Pacific [*Carter et al.*, 2008]. In addition to the $\delta^{13}C$ records, *N. dutertrei* εNd data from ODP 1240 indicate increased influence of the Southern Ocean between 11 and 8 kyr [*Pena et al.*, 2013]. The $\delta^{13}C$ data and neighboring εNd data support the connection between the EEP subsurface and the Southern Ocean.

5.2 Mechanism to explain warm early Holocene SAMW

A current hypothesis for the rise in deglacial CO_2 is a poleward SWW shift which caused Antarctica to warm and increased upwelling in the Southern Ocean [*Anderson et al.*, 2009]. The rise of CO_2 is thought to occur in two steps, the first during Heinrich stadial 1 (18-14.7 kyr) and the second between 13 and 9 kyr. We suggest that the warmth in the early Holocene was related to the aforementioned southward position of the SWW and that the subsequent cooling was caused by a northward shift of the SWW. Southern Ocean temperature records and precipitation records from the Chilean margin have also been used to argue for a more poleward position of the SWW in the early Holocene and an equatorward shift between 9-8 kyr [*Lamy et al.*, 2010; *Shevenell et al.*, 2011]. Modeling studies indicate that increased freshwater flux may be responsible for the northward shift in the winds [*Mathiot et al.*, 2013].

Proxy data suggest that the southward migration of the SWW caused a southward displacement in the position of the STF [*Bostock et al.*, 2013], possibly allowing more warm subtropical water to reach the SAMW formation region and thus warming SAMW. Observations have shown that eddies are important in transporting warm, subtropical waters into SAMW formation regions [*Hartin et al.*, 2011]. The difference between the *N. dutertrei* $\delta^{18}O_C$ and Mg/Ca estimates of the temperature change in the early Holocene implies that the thermostad water was warmer and saltier during the early Holocene. This is also coherent with greater influence of subtropical water. Thus if the STF was shifted poleward, this would allow for a greater transport of warm subtropical water via eddies to enter the SAMW formation region thereby likely increasing the temperature of the subducted SAMW, which eventually reached the equatorial Pacific thermostad.

The influence of SAMW on the thermostad may be unique to the early Holocene. Although the $\delta^{13}C$ records suggest Southern Ocean influence throughout the Holocene, the εNd from ODP1240 indicates a greater influence of Southern Ocean in the EEP only between 10 and 8 kyr [*Pena et al.*, 2013]. These proxy data agree with models, which predict that stronger and more poleward SWW increase the winter mixed layer causing enhanced subduction of SAMW, particularly in the Pacific basin [*Downes et al.*, 2011]. The early Holocene change in the southern high latitudes was robust and a rather large transition in the climate system that had influence as far north as the equatorial Pacific, likely as a result of changes in ocean-atmosphere dynamics, not necessarily orbital forcing as has been proposed previously [*Rosenthal et al.*, 2013; *Shevenell et al.*, 2011].

5.3 Implications for Ocean Heat Content in the Holocene

Our new records provide evidence for the early Holocene contribution of high latitudes climate to the heat content of the EEP thermostad as a result of post glacial frontal movements in the Southern Hemisphere. Intermediate water (600-900 m) temperatures from the Indonesia Throughflow (ITF) are also warmer between 10 and 8 kyr but by only ~1˚C rather than by ~2˚C (Figure 8) [*Rosenthal et al.*, 2013]. This implies that southern high latitude climate signals affected AAIW as well as SAMW. After 8 kyr, the two records diverge with the ITF temperature record showing stronger cooling of about ~1.5˚C, while the EEP temperature records show significant centennial variability but no long-term trend (Figure 8). The difference after 8 kyr may result from a weaker influence of the Southern Ocean in the EEP [*Pena et al.*, 2013], a greater subtropical influence in the EEP and/or Northern Hemisphere influence in the ITF region.

The early Holocene temperature anomalies in the subsurface of the EEP do not affect the surface with the same magnitude. The thermostad water is thought to join the Peru-Chile Undercurrent [*Chaigneau et al.*, 2013] and eventually to upwell in the cold tongue. A high resolution SST reconstruction from the cold tongue at 14˚S does show temperatures that are ~0.5˚C higher in between 9.5 and 8.9 kyr (Figure 8) [*Chazen et al.*, 2009]. The warm SST may be a result of the surfacing of the temperature signal from the thermostad, however, it is not as strong as a signal as is seen in the subsurface nor is it unique to the early Holocene. The weak SST signal may result from the thermostad temperature signal being dissipated by subsurface eddies which occur in the Peru-Chile Undercurrent [*Johnson and McTaggart*, 2010]. The weak surface expression implies that the temperature signal from the southern high latitudes largely remains sequestered from the surface once it is subducted, supporting the argument that changes in the interior OHC may help distribute heat associated with climate change [*Levitus et al.*, 2012; *Rosenthal et al.*, 2013].

6. Conclusion

We've reconstructed Holocene temperatures of the EEP thermostad, the water mass of relatively uniform temperature below the Pacific Equatorial Undercurrent. Based on the comparison with ice core, SST and precipitation records from the Southern Hemisphere, we suggest that warm thermostad temperature in the early Holocene, prior to 8 kyr, likely originated in the southern high latitudes. SAMW is the most probable source of the warm early Holocene thermostad temperature because other EEP thermostad source regions do not show a similar temperature pattern. Furthermore, the link to the Southern Ocean source region is supported by the $\delta^{13}C$ records as well as the εNd record in a neighboring core. We hypothesize that the early Holocene warmth in the EEP thermostad, was caused by a more southerly position of the SWW, which caused increased influence of warm, salty subtropical water into the SAMW formation region. A similar mechanism potentially has implications for future climate change.

The SWW have become stronger and shifted poleward in response to a positive Southern Annular Mode over the past 50 years [*Thompson et al.*, 2011]. Similar to the early Holocene, chlorofluorocarbon measurements imply increased transport of SAMW for the last two decades [*Waugh et al.*, 2013]. Further recent observations from Argo floats indicate that water sourced from the Southern Ocean are one of the largest contributors to a recent increase in OHC in the southern subtropical gyre [*Roemmich et al.*, 2015]. Although these observations support the possibility that changes in the SWW affect OHC, the transport time to the EEP thermostad is greater than 50 years [*Qu et al.*, 2009] indicating that it is too soon to know if the current changes in the SWW will reach the EEP thermostad. Nonetheless, both this study and current observations provide evidence that ocean-atmosphere dynamics in the southern high latitudes are important in determining OHC on various timescales and may help sequester heat in the future.

Acknowledgements

We would like to thank the captain and crew of the Knorr for all their help in retrieving the core and samples used in this paper. We would also like to thank Athena Fu, Joshua Epstein and Elia Claros for their help in preparing foraminifera samples and Stella Woodard and Elisabeth Sikes for insightful discussions. Additionally two anonymous reviewers provided helpful critiques of a previous draft to make this paper better. Support for this project came from NSF award OCE 1003400 to YR.

References

Anand, P., Elderfield, H., and Conte, M. H., 2003. Calibration of Mg/Ca thermometry in planktonic foraminifera from a sediment trap time series. *Paleoceanography* **18**, doi: 10.1029/2002PA000846.

Anderson, R. F., Ali, S., Bradtmiller, L. I., Nielsen, S. H. H., Fleisher, M. Q., Anderson, B. E., and Burckle, L. H., 2009. Wind-Driven Upwelling in the Southern Ocean and the Deglacial Rise in Atmospheric CO_2. *Science* **323**, 1443-1448, doi: 10.1126/science.1167441.

Balmaseda, M. A., Trenberth, K. E., and Kallen, E., 2013. Distinctive climate signals in reanalysis of global ocean heat content. *Geophysical Research Letters* **40**, 1754-1759, doi: 10.1002/grl.50382.

Bard, E., Hamelin, B., and Delanghe-Sabatier, D., 2010. Deglacial Meltwater Pulse 1B and Younger Dryas Sea Levels Revisited with Boreholes at Tahiti. *Science* **327**, 1235-1237, doi: 10.1126/science.1180557.

Bemis, B. E., Spero, H. J., and Thunell, R. C., 2002. Using species-specific paleotemperature equations with foraminifera: a case study in the Southern California Bight. *Marine Micropaleontology* **46**, 405-430, doi:10.1016/S0377-8398(02)00083-X.

Bostock, H. C., Barrows, T. T., Carter, L., Chase, Z., Cortese, G., Dunbar, G. B., Ellwood, M., Hayward, B., Howard, W., Neil, H. L., Noble, T. L., Mackintosh, A., Moss, P. T., Moy, A. D., White, D., Williams, M. J. M., and Armand, L. K., 2013. A review of the Australian-New Zealand sector of the Southern Ocean over the last 30 ka (Aus-INTIMATE project). *Quaternary Science Reviews* **74**, 35-57, doi:10.1016/j.quascirev.2012.07.018.

Bryan, S. P. and Marchitto, T. M., 2008. Mg/Ca-temperature proxy in benthic foraminifera: New calibrations from the Florida Straits and a hypothesis regarding Mg/Li. *Paleoceanography* **23**, PA2220, DOI: 10.1029/2007PA001553.

Cai, W. J., Cowan, T., Godfrey, S., and Wijffels, S., 2010. Simulations of Processes Associated with the Fast Warming Rate of the Southern Midlatitude Ocean. *Journal of Climate* **23**, 197-206, doi:10.1175/2009JCLI3081.1

Carter, L., Manighetti, B., Ganssen, G., and Northcote, L., 2008. Southwest Pacific modulation of abrupt climate change during the Antarctic Cold Reversal-Younger Dryas, *Palaeogeography, Palaeoclimatology, Palaeoecology* **260**, 284-298, doi:10.1016/j.palaeo.2007.08.013.

Chaigneau, A., Dominguez, N., Eldin, G., Vasquez, L., Flores, R., Grados, C., and Echevin, V., 2013. Near-coastal circulation in the Northern Humboldt Current System from shipboard ADCP data. *Journal of Geophysical Research: Oceans* **118**, 5251-5266, doi: 10.1002/jgrc.20328.

Chazen, C. R., Altabet, M. A., and Herbert, T. D., 2009. Abrupt mid-Holocene onset of centennial-scale climate variability on the Peru-Chile Margin. *Geophysical Research Letters* **36,** doi: 10.1029/2009GL039749.

Downes, S. M., Budnick, A. S., Sarmiento, J. L., and Farneti, R., 2011. Impacts of wind stress on the Antarctic Circumpolar Current fronts and associated subduction. *Geophysical Research Letters* **38**, L11605, doi: 10.1029/2011GL047668.

Elderfield, H., Greaves, M., Barker, S., Hall, I. R., Tripati, A., Ferretti, P., Crowhurst, S., Booth, L., and Daunt, C., 2010. A record of bottom water temperature and seawater δ^{18}O for the Southern Ocean over the past 440 kyr based on Mg/Ca of benthic foraminiferal Uvigerina spp. *Quaternary Science Reviews* **29**, 160-169, doi:10.1016/j.quascirev.2009.07.013.

England, M. H., McGregor, S., Spence, P., Meehl, G. A., Timmermann, A., Cai, W., Gupta, A. S., McPhaden, M. J., Purich, A., and Santoso, A., 2014. Recent intensification of wind-driven circulation in the Pacific and the ongoing warming hiatus. *Nature Climate Change* **4**, 222-227, doi:10.1038/nclimate2106.

Fairbanks, R. G., Mortlock, R. A., Chiu, T.-C., Cao, L., Kaplan, A., Guilderson, T. P., Fairbanks, T. W., Bloom, A. L., Grootes, P. M., and Nadeau, M.J., 2005. Radiocarbon calibration curve spanning 0 to 50,000 years BP based on paired 230Th/234U/238U and 14C dates on pristine corals. *Quaternary Science Reviews* **24**, 1781-1796, doi:10.1016/j.quascirev.2005.04.007.

Hartin, C. A., Fine, R. A., Sloyan, B. M., Talley, L. D., Chereskin, T. K., and Happell, J., 2011. Formation rates of Subantarctic mode water and Antarctic intermediate water within the South Pacific. *Deep Sea Research Part I: Oceanographic Research Papers* **58**, 524-534, doi:10.1016/j.dsr.2011.02.010.

Haug, G. H., Hughen, K. A., Sigman, D. M., Peterson, L. C., and Röhl, U., 2001. Southward Migration of the Intertropical Convergence Zone Through the Holocene. *Science* **293**, 1304-1308, doi: 10.1126/science.1059725.

Herraiz-Borreguero, L. and Rintoul, S. R., 2011. Subantarctic mode water: distribution and circulation. *Ocean Dynamics* **61**, 103-126, doi: 10.1007/s10236-010-0352-9.

Johnson, G. C. and McTaggart, K. E., 2010. Equatorial Pacific 13 degrees C Water Eddies in the Eastern Subtropical South Pacific Ocean. *Journal of Physical Oceanography* **40**, 226-236, doi:10.1175/2009JPO4287.1.

Jones, D. C., Ito, T., and Lovenduski, N. S., 2011. The transient response of the Southern Ocean pycnocline to changing atmospheric winds. *Geophysical Research Letters* **38,** doi:10.1029/2011GL048145.

Kaiser, J., Lamy, F., and Hebbeln, D., 2005. A 70-kyr sea surface temperature record off southern Chile (Ocean Drilling Program Site 1233). *Paleoceanography* **20**, doi: 10.1029/2005PA001146.

Koutavas, A. and Sachs, J. P., 2008. Northern timing of deglaciation in the eastern equatorial Pacific from alkenone paleothermometry. *Paleoceanography* **23**, PA4205, 10.1029/2008PA001593.

Lamy, F., Kilian, R., Arz, H. W., Francois, J. P., Kaiser, J., Prange, M., and Steinke, T., 2010. Holocene changes in the position and intensity of the southern westerly wind belt. *Nature Geoscience* **3**, 695-699, doi:10.1038/ngeo959.

LeGrande, A. N. and Schmidt, G. A., 2006. Global gridded data set of the oxygen isotopic composition in seawater. *Geophysical Research Letters* **33**, L12604, doi:10.1029/2006GL026011.

Lighty, R. G., Macintyre, I. G., and Stuckenrath, R., 1982. Acropora Palmata Reef Framework: A Reliable Indicator of Sea Level in the Western Atlantic for the Past 10,000 Years. *Coral Reefs* **1**, 125-130, doi:10.1007/BF00301694.

Marchitto, T. M., Muscheler, R., Ortiz, J. D., Carriquiry, J. D., and van Geen, A., 2010. Dynamical Response of the Tropical Pacific Ocean to Solar Forcing During the Early Holocene. *Science* **330**, 1378-1381, doi: 10.1126/science.1194887.

Marchitto, T.M., Curry, W.B., Lynch-Stieglitz, J., Bryan, S.P., Cobb, K.M., Lund, D.C., 2014. Improved oxygen isotope temperature calibrations for cosmopolitan benthic foraminifera. *Geochimica et Cosmochimica Acta* **230**, 1-11, doi:10.1016/j.gca2013.12.034.

Martin, P. A., Lea, D. W., Rosenthal, Y., Shackleton, N. J., Sarnthein, M., and Papenfuss, T., 2002. Quaternary deep sea temperature histories derived from benthic foraminiferal Mg/Ca. *Earth and Planetary Science Letters* **198**, 193-209, doi:10.1016/S0012-821X(02)00472-7.

Masson-Delmotte, V., Buiron, D., Ekaykin, A., Frezzotti, M., Gallee, H., Jouzel, J., Krinner, G., Landais, A., Motoyama, H., Oerter, H., Pol, K., Pollard, D., Ritz, C., Schlosser, E., Sime, L. C., Sodemann, H., Stenni, B., Uemura, R., and Vimeux, F., 2011. A comparison of the present and last interglacial periods in six Antarctic ice cores. *Climate of the Past* **7**, 397-423, doi:10.5194/cp-7-397-2011.

Mathiot, P., Goosse, H., Crosta, X., Stenni, B., Braida, M., Renssen, H., Van Meerbeeck, C. J., Masson-Delmotte, V., Mairesse, A., and Dubinkina, S., 2013. Using data assimilation to investigate the causes of Southern Hemisphere high latitude cooling from 10 to 8 ka BP. *Climate of the Past* **9**, 887-901, doi: 10.5194/cp-9-887-2013.

Mohtadi, M., Rossel, P., Lange, C. B., Pantoja, S., Boning, P., Repeta, D. J., Grunwald, M., Lamy, F., Hebbeln, D., and Brumsack, H. J., 2008. Deglacial pattern of circulation and marine productivity in the upwelling region off central-south Chile. *Earth and Planetary Science Letters* **272**, 221-230, doi:10.1016/j.epsl.2008.04.043.

Mulvaney, R., Abram, N. J., Hindmarsh, R. C. A., Arrowsmith, C., Fleet, L., Triest, J., Sime, L. C., Alemany, O., and Foord, S., 2012. Recent Antarctic Peninsula warming relative to Holocene climate and ice-shelf history. *Nature* **489**, 141-U204, doi:10.1038/nature11391.
Pahnke, K. and Sachs, J. P., 2006. Sea surface temperatures of southern midlatitudes 0–160 kyr B.P. *Paleoceanography* **21**, PA2003, doi: 10.1029/2005PA001191.
Peltier, W. R. and Fairbanks, R. G., 2006. Global glacial ice volume and Last Glacial Maximum duration from an extended Barbados sea level record. *Quaternary Science Reviews* **25**, 3322-3337, 10.1029/2008PA001620.
Pena, L. D., Cacho, I., Ferretti, P., and Hall, M. A., 2008. El Nino-Southern Oscillation-like variability during glacial terminations and interlatitudinal teleconnections. *Paleoceanography* **23**, PA3101, doi: 10.1029/2008PA001620
Pena, L. D., Goldstein, S. L., Hemming, S. R., Jones, K. M., Calvo, E., Pelejero, C., and Cacho, I., 2013. Rapid changes in meridional advection of Southern Ocean intermediate waters to the tropical Pacific during the last 30kyr. *Earth and Planetary Science Letters* **368**, 20-32, doi:10.1016/j.epsl.2013.02.028.
Qu, T. D., Gao, S., Fukumori, I., Fine, R. A., and Lindstrom, E. J., 2009. Origin and Pathway of Equatorial 13 degrees C Water in the Pacific Identified by a Simulated Passive Tracer and Its Adjoint. *Journal of Physical Oceanography* **39**, 1836-1853, doi:10.1175/2009JPO4045.1.
Qu, T. D., Gao, S., Fukumori, I., Fine, R. A., and Lindstrom, E. J., 2010. The Obduction of Equatorial 13°C Water in the Pacific Identified by a Simulated Passive Tracer. *Journal of Physical Oceanography*, **40**, 2282–2297, doi: 10.1175/2010JPO4358.1.
Rincon-Martinez, D., Steph, S., Lamy, F., and Mix, A., 2011. Tracking the equatorial front in the eastern equatorial Pacific Ocean by the isotopic and faunal composition of planktonic foraminifera. *Marine Micropaleontology* **79**, 24-40, doi: 10.1029/2009PA001868.
Roemmich, D., Church, J., Gilson, J., Monselesan, D., Sutton, P., and Wijffels, S., 2015. Unabated planetary warming and its ocean structure since 2006. *Nature Climate Change* **5**, 240-245, doi:10.1038/nclimate2513.
Rosenthal, Y., Boyle, E. A., and Labeyrie, L., 1997. Last Glacial Maximum paleochemistry and deepwater circulation in the Southern Ocean: Evidence from foraminiferal cadmium. *Paleoceanography* **12**, 787-796, doi: 10.1029/97PA02508.
Rosenthal, Y., Linsley, B. K., and Oppo, D. W., 2013. Pacific Ocean Heat Content During the Past 10,000 Years. *Science* **342**, 617-621, doi: 10.1126/science.124083.
Rowe, G. D., Firing, E., and Johnson, G. C., 2000. Pacific equatorial subsurface countercurrent velocity, transport, and potential vorticity. *Journal of Physical Oceanography* **30**, 1172-1187.
Shevenell, A. E., Ingalls, A. E., Domack, E. W., and Kelly, C., 2011. Holocene Southern Ocean surface temperature variability west of the Antarctic Peninsula (vol 470, pg 250, 2011). *Nature* **472**, doi:10.1038/nature09751
Sirocko, F., Sarnthein, M., Erlenkeuser, H., Lange, H., Arnold, M., and Duplessy, J. C., 1993. Century-scale events in monsoonal climate over the past 24,000 years. *Nature* **364**, 322-324, doi:10.1038/364322a0.
Spero, H. J. and Lea, D. W., 2002. The Cause of Carbon Isotope Minimum Events on Glacial Terminations. *Science* **296**, 522-525, doi: 0.1126/science.1069401.
Thompson, D. W. J., Solomon, S., Kushner, P. J., England, M. H., Grise, K. M., and Karoly, D. J., 2011. Signatures of the Antarctic ozone hole in Southern Hemisphere surface climate change. *Nature Geoscience* **4**, 741-749, doi:10.1038/ngeo1296.
Toggweiler, J. R., Dixon, K., and Broecker, W. S., 1991. The Peru Upwelling and the Ventilation of the South Pacific Thermocline. *J. Geophys. Res.* **96**, 20467-20497, doi: 10.1029/91JC02063.
Tsuchiya, M., 1981. The Origin of the Pacific Equatorial 13˚C Water. *Journal of Physical*

Oceanography **11**, 794-812.
Waugh, D. W., Primeau, F., DeVries, T., and Holzer, M., 2013. Recent Changes in the Ventilation of the Southern Oceans. *Science* **339**, 568-570, doi: 10.1126/science.1225411.

Table Caption

Table 1. The radiocarbon dates for CDH23. A reservoir age of 500 years has been subtracted from carbon-14 year values shown. The radiocarbon year was converted to calendar year using the Fairbanks et al. [2005] calibration.

Figure Captions

Figure 1. Neutral density isopycnals are contoured on top of temperature (color bar) from across the Pacific centered at 3-5˚S. The thermostad ranges from 11-14˚C and 26.2-26.6 kg/m^3. The yellow circle at right indicates the approximate depth of calcification for *N. dutertrei* and the white circle below it indicates the depth of the core-top *Uvigerina* calcification. The image was made with Ocean Data View (http://odv.awi.de/) using the data from World Ocean Atlas 2009.

Figure 2. (A) Location of core site (yellow circle) and location of core ODP 1240 (2941 m water depth). (B) Expanded view of light blue box in (A), showing detail of bathymetry in region of core location. The shelf-slope is approximately 60 km wide, extends to a depth of about 400 m and is bounded by a steep slope with a gradient of 70 m per km. Figures generated using geomapapp.org.

Figure 3. Calendar year estimated from *N. dutertrei* radiocarbon dates using a 500 year reservoir age and the Fairbanks et al. [2005] calibration. The error bars on the ages are indicated but are smaller than symbols in most cases. The sedimentation rate is relatively constant throughout the core.

Figure 4. Core top *N. dutertrei* $\delta^{18}O_C$ (black markers) are plotted on water column profiles of $\delta^{18}O_c$ which were converted from discrete $\delta^{18}O_{SW}$ samples taken during the cruise (green) and derived from the $\delta^{18}O$ model of LeGrand and Schmidt [2006] (red). The $\delta^{18}O_{SW}$ values were converted to $\delta^{18}O_C$ using the Marchitto et al. [2014] equation. The open black symbols represent the $\delta^{18}O_C$ for the different size fractions of *N. dutertrei*. The calcification depth for the size the 355-425 µm *N. dutertrei* (open circle) was determined to be between 100-130 m based on where the $\delta^{18}O_C$ of *N. dutertrei* and $\delta^{18}O_C$ converted from sea water overlap. Individual core top *N. dutertrei* Mg/Ca temperature estimates (grey open circles) and the average are plotted on a temperature profile from World Ocean Atlas 2009. The vertical error bars represent the estimated depth habitat of 355-425 µm *N. dutertrei*.

Figure 5. *N. dutertrei* (blue) and *Uvigerina* (black) individual data (thin line) and 3-point running average (thick line) from the Holocene. (A) Subthermocline temperature reconstructions are estimated from Mg/Ca of *N. dutertrei* using the Anand et al. [2003] multi species calibration. $\delta^{18}O_C$ (red dashed line) has been corrected for sea level (refer to text). (B) Same as A, but for *Uvigerina* and temperature are estimated using a modified calibration equation from Bryan and Marchitto [2008] and temperature is corrected for sea level. (C) *N. dutertrei* and *Uvigerina* $\delta^{13}C$ records

Figure 6. Southern Hemisphere high latitude temperature and precipitation records plotted along with *Uvigerina* and *N. dutertrei* temperature anomalies from the EEP. The yellow shaded area is the period of early Holocene warmth. (A) Antarctic temperature records from and Empirical Orthogonal Function (EOF) of 5 ice core δ^{18}O records (black line) [*Masson-Delmotte et al.*, 2011] and James Ross ice core δD (blue line) *[Mulvaney et al., 2012]* (B) Ocean temperature records (0-150 m) from the Pacific sector of the Southern Ocean (black line, left axis) [*Shevenell et al.*, 2011], SST from MD97 2021 (45˚S, 174˚E) (red line, right axis) [*Pahnke and Sachs*, 2006] and SST from ODP 1233 (41˚S, 74˚W) (blue line, right axis) [*Kaiser et al.*, 2005] (C) Corg and siliciclastic accumulation rates as proxies for precipitation from the Chilean Fjords (53˚S) [*Lamy et al.*, 2010] (D) *N. dutertrei* (blue) and *Uvigerina* (black) temperature reconstructions from the EEP (this study). Note the different temperature scales on the axes

Figure 7. Planktonic δ^{13}C records from various locations around the globe show a similar increase in δ^{13}C values until around 6 kyr. Grey line *[Sirocko et al., 1993]*, orange line [*Carter et al.*, 2008], green line [*Pena et al.*, 2008], *N. dutertrei* (this study) (blue line). *Uvigerina* (this study) (black line) is the only benthic specie.

Figure 8. (A) SST temperature records from 14˚S, 74˚W [*Chazen et al.*, 2009] plotted along with (B) the EEP *N. dutertrei* (blue) and *Uvigerina* (black) and (C) the ITF 600-900 m [*Rosenthal et al.*, 2013] temperature anomalies. The ITF and the EEP subsurface temperature records are warmer during the early Holocene, but the signal is not as pronounced in the SST record from the cold tongue.

Graphical Abstract (for review)

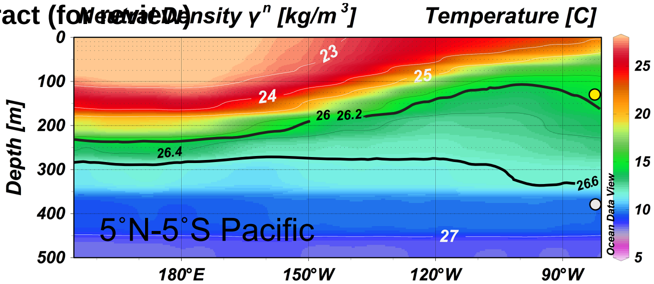

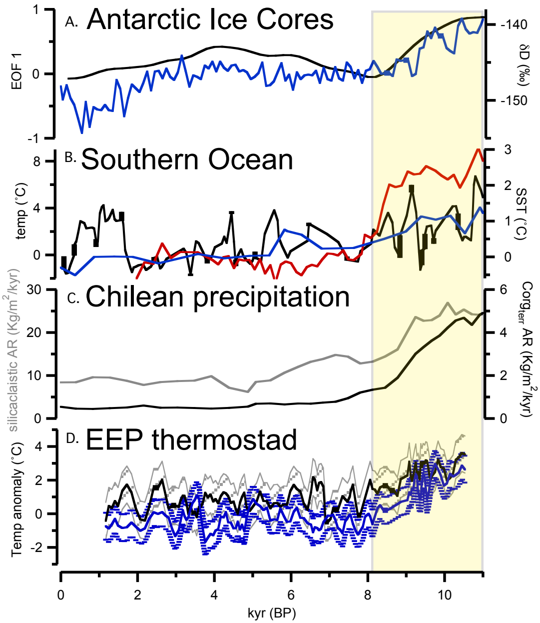

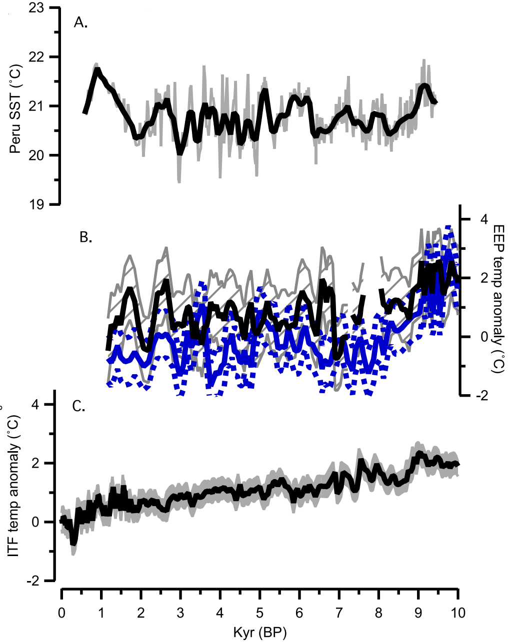

Figure 1

FIGURES

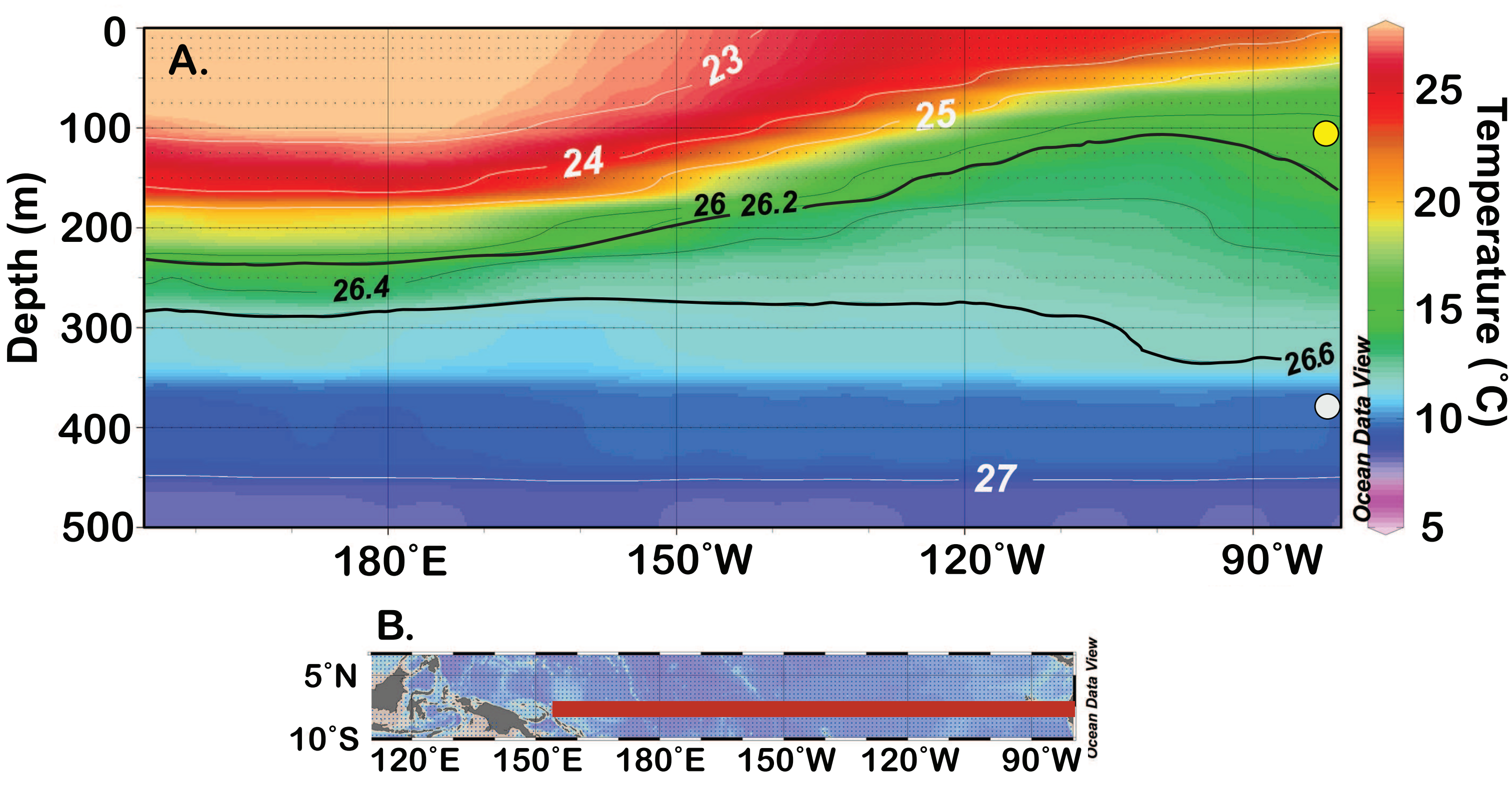

Figure 2

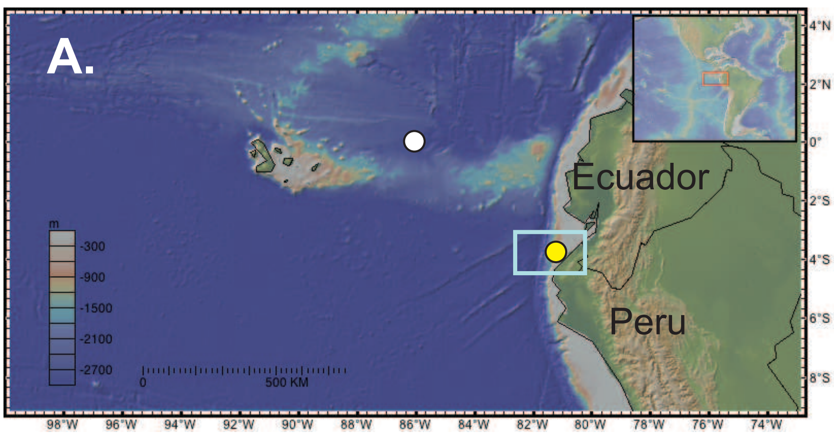

A.
Ecuador
Peru
m
-300
-900
-1500
-2100
-2700
0
500 KM
4°N
2°N
0°
2°S
4°S
6°S
8°S
98°W
96°W
94°W
92°W
90°W
88°W
86°W
84°W
82°W
80°W
78°W
76°W
74°W

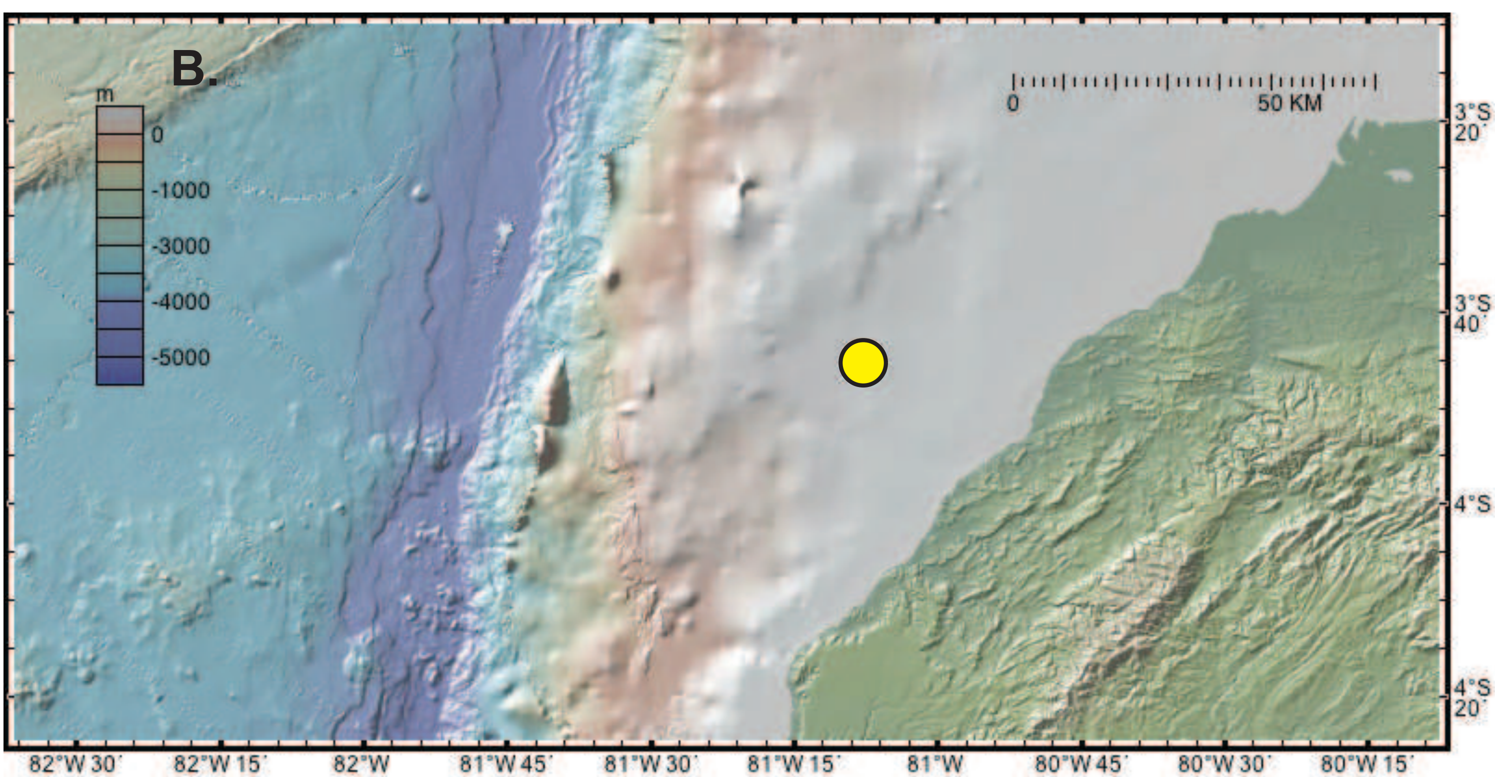

B.
m
0
-1000
-3000
-4000
-5000
0
50 KM
3°S 20'
3°S 40'
4°S
4°S 20'
82°W 30'
82°W 15'
82°W
81°W 45'
81°W 30'
81°W 15'
81°W
80°W 45'
80°W 30'
80°W 15'

Figure 3

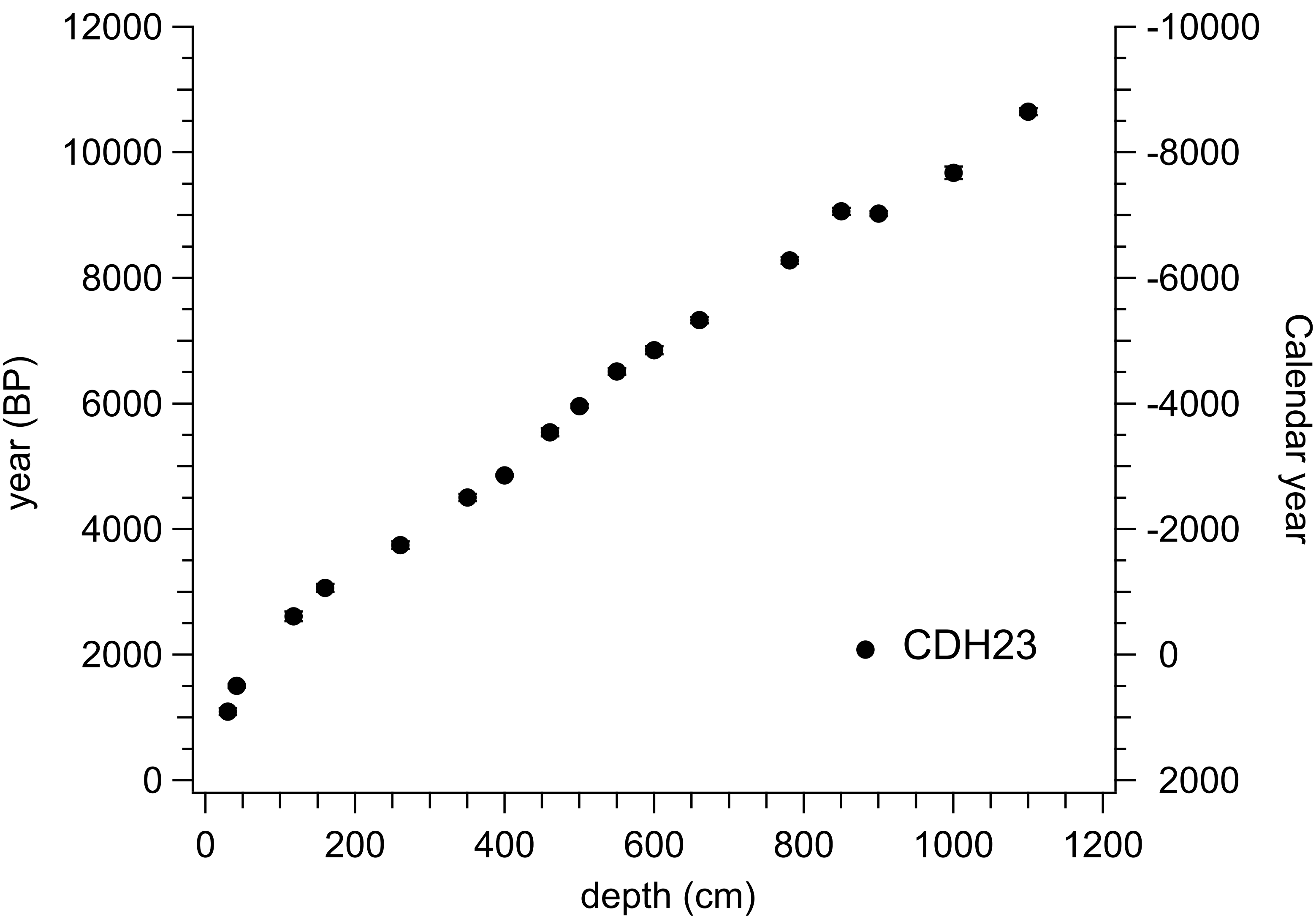

12000
10000
8000
6000
4000
2000
0
year (BP)
-10000
-8000
-6000
-4000
-2000
0
2000
Calendar year
CDH23
0
200
400
600
800
1000
1200
depth (cm)

Figure 4

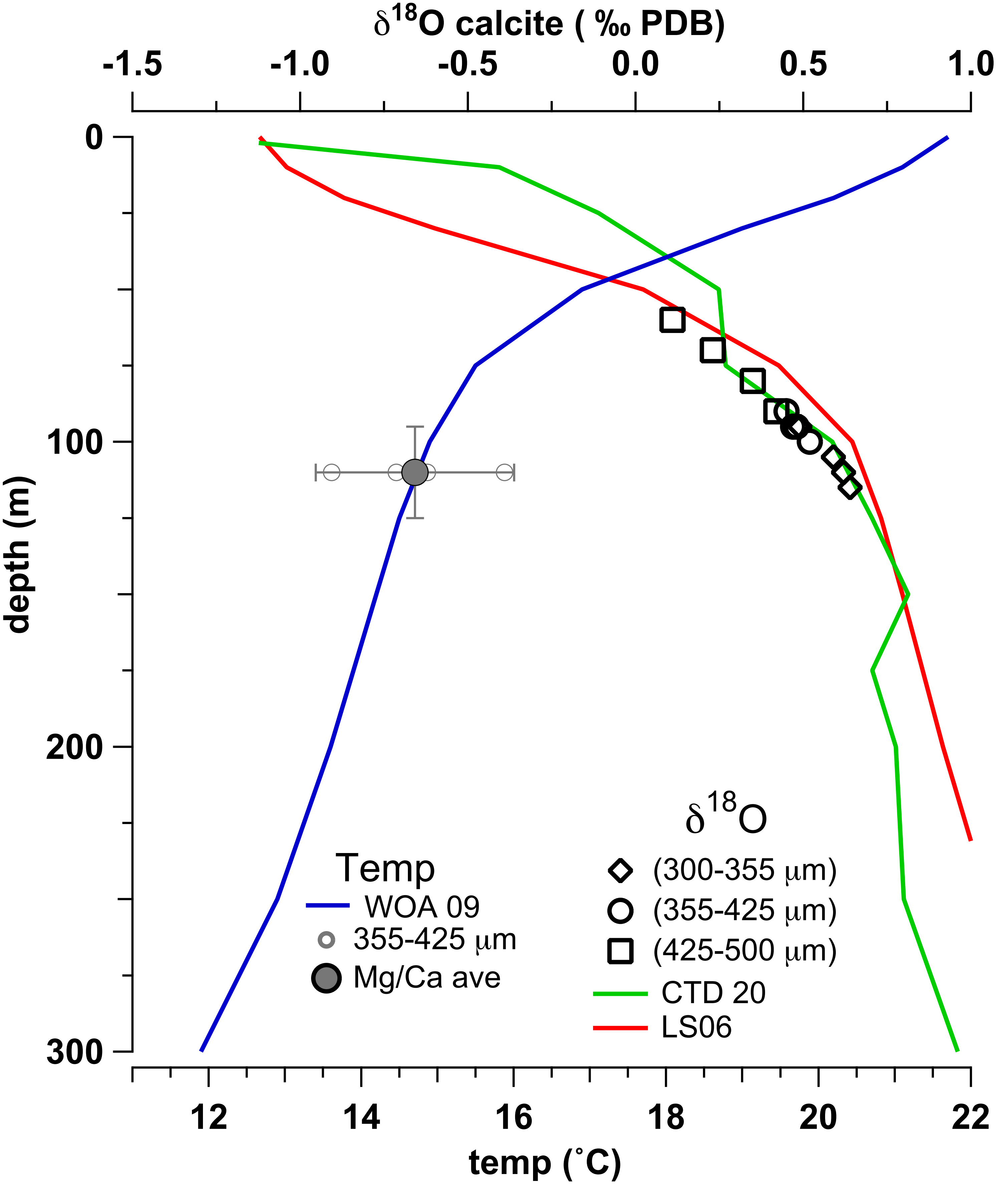
δ18O calcite (‰ PDB)
-1.5
-1.0
-0.5
0.0
0.5
1.0
0
100
200
300
depth (m)
12
14
16
18
20
22
temp (˚C)
Temp
WOA 09
355-425 μm
Mg/Ca ave
δ18O
(300-355 μm)
(355-425 μm)
(425-500 μm)
CTD 20
LS06

Figure 5

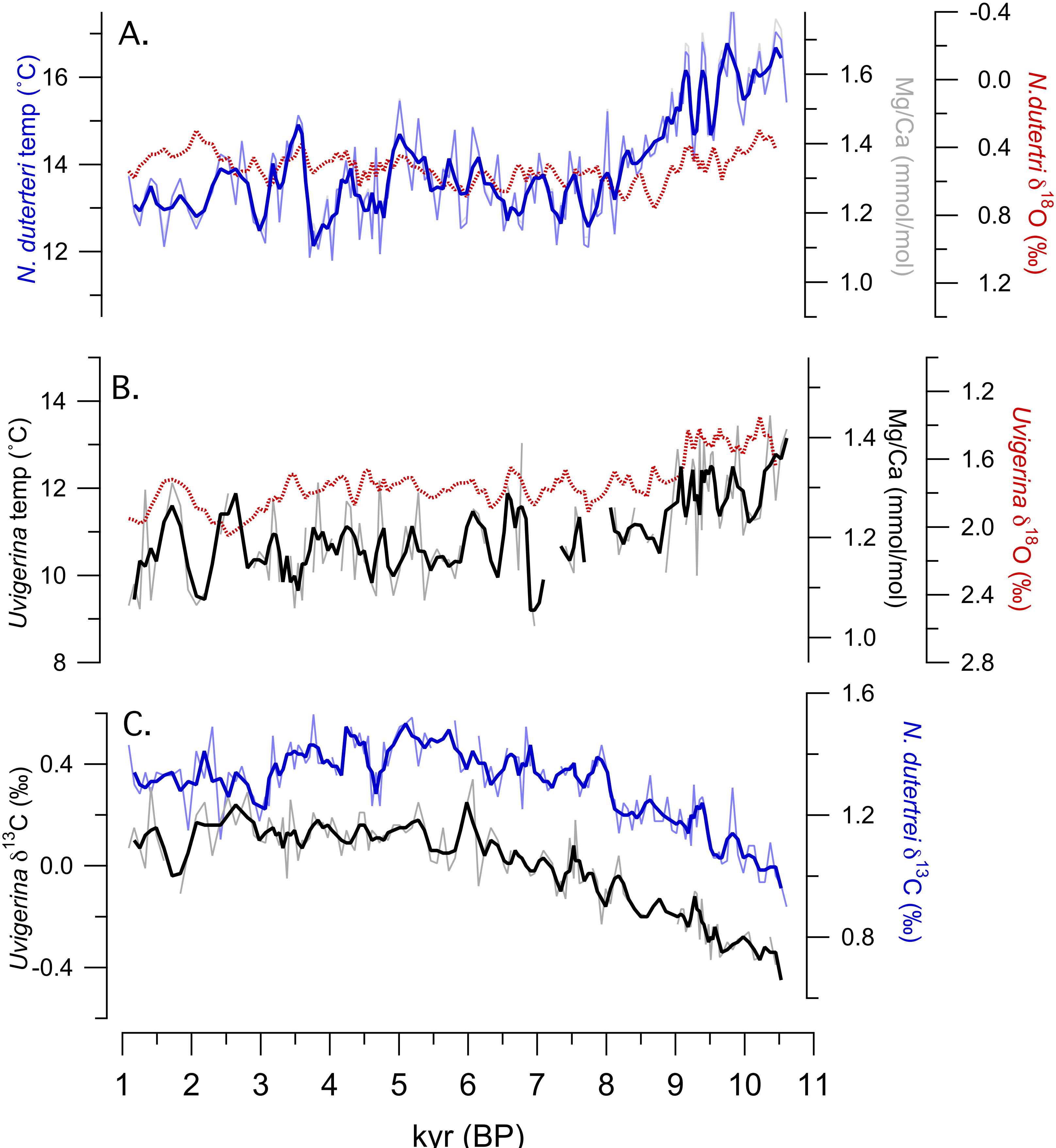

A.
N. duterteri temp (˚C)
16
14
12
1.6
1.4
1.2
1.0
Mg/Ca (mmol/mol)
-0.4
0.0
0.4
0.8
1.2
N.dutertri δ18O (‰)
B.
Uvigerina temp (˚C)
14
12
10
8
Mg/Ca (mmol/mol)
1.4
1.2
1.0
1.2
1.6
2.0
2.4
2.8
Uvigerina δ18O (‰)
C.
Uvigerina δ13C (‰)
0.4
0.0
-0.4
1.6
1.2
0.8
N. dutertrei δ13C (‰)
1
2
3
4
5
6
7
8
9
10
11
kyr (BP)

Figure 6

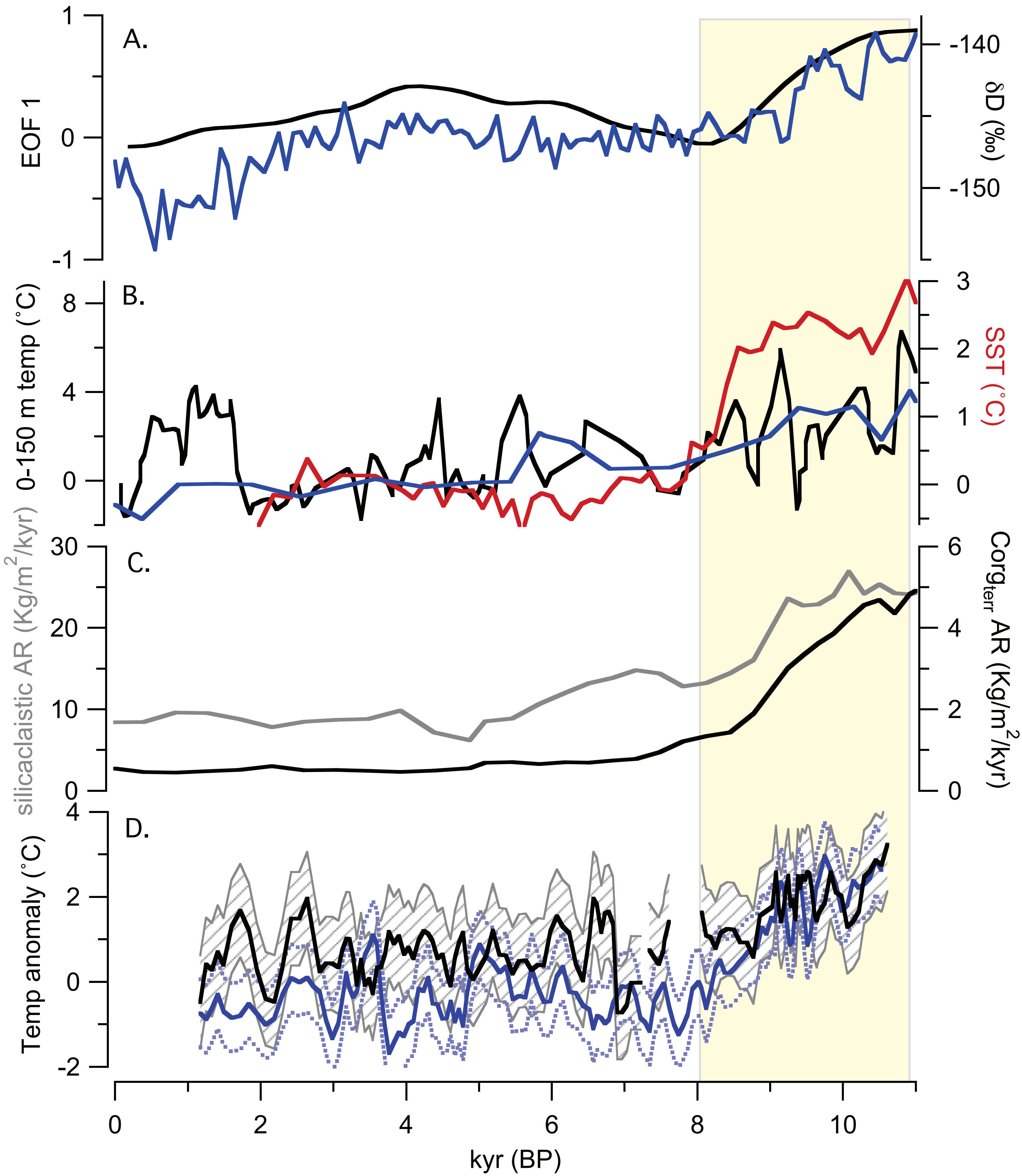

A.
EOF 1
δD (‰)
1
0
-1
-140
-150
B.
0-150 m temp (˚C)
SST (˚C)
8
4
0
3
2
1
0
C.
silicaclaistic AR (Kg/m2/kyr)
Corgterr AR (Kg/m2/kyr)
30
20
10
0
6
4
2
0
D.
Temp anomaly (˚C)
4
2
0
-2
0
2
4
6
8
10
kyr (BP)

Figure 7

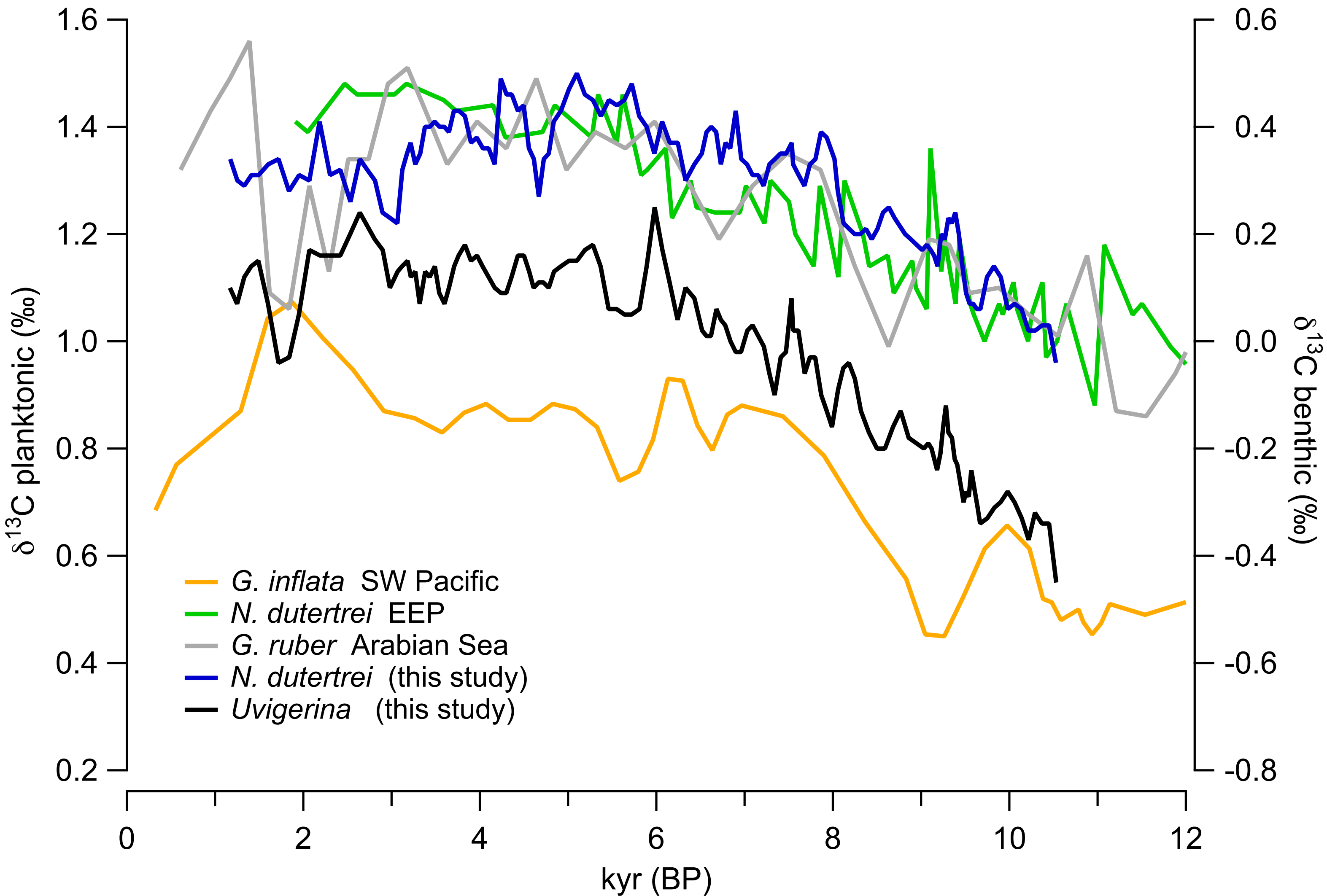

1.6
1.4
1.2
1.0
0.8
0.6
0.4
0.2
δ13C planktonic (‰)
0.6
0.4
0.2
0.0
-0.2
-0.4
-0.6
-0.8
δ13C benthic (‰)
0
2
4
6
8
10
12
kyr (BP)
G. inflata SW Pacific
N. dutertrei EEP
G. ruber Arabian Sea
N. dutertrei (this study)
Uvigerina (this study)

Figure 8

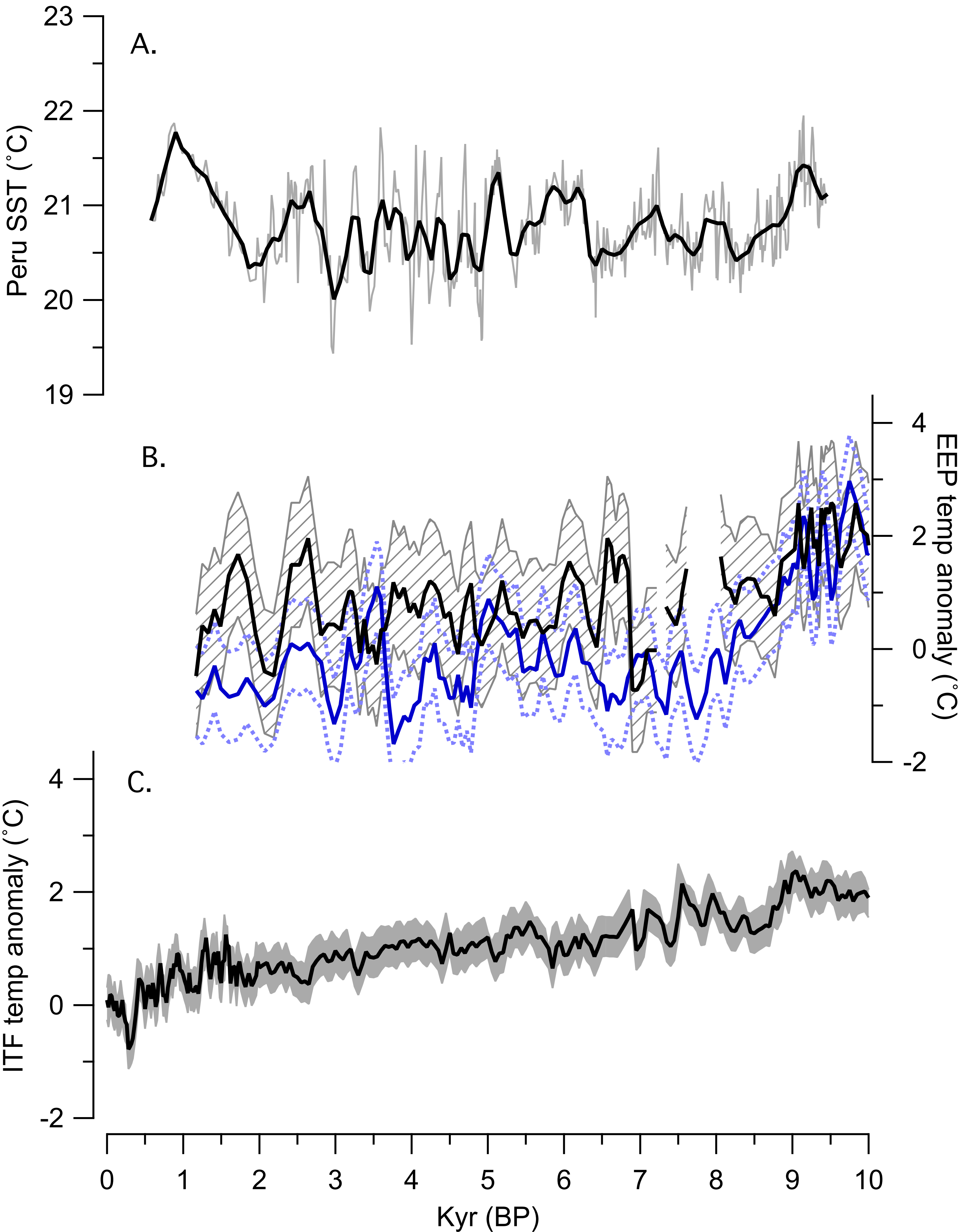

A.
B.
C.
Peru SST (˚C)
23
22
21
20
19
EEP temp anomaly (˚C)
4
2
0
-2
ITF temp anomaly (˚C)
4
2
0
-2
0
1
2
3
4
5
6
7
8
9
10
Kyr (BP)

Table 1

Core	ID	Depth (cm)	Carbon-14 year ± 1 sigma	calendar year ± 1 sigma
CDH23	OS- 77623	30	1180±40	1091±56
CDH23	OS-101833	42	1610±20	1505±33
CDH23	OS-101834	118	2500±20	2611±76
CDH23	OS 77579	160	2920±35	3061±64
CDH23	OS-77576	260.5	3480±35	3745±58
CDH23	OS-77575	350.5	4040±40	4504±61
CDH23	OS-84123	400	4300±35	4853±20
CDH23	OS- 77546	460.5	4790±50	5540±62
CDH23	OS-84122	500	5220±30	5958±33
CDH23	OS-84108	550	5730±35	6510±49
CDH23	OS-84168	600	6010±45	6847±62
CDH23	OS-77574	660.5	6400±40	7326±49
CDH23	OS-84121	781	7450±40	8281±57
CDH23	OS-77580	850.25	8140±45	9062±56
CDH23	OS-84120	900	8100±45	9023±41
CDH23	OS-77547	1000.25	8720±60	9675±102
CDH23	OS-84115	1100	9420±40	10648±54